J. Chem. Chem. Eng. 8 (2014) 1026-1035
doi: 10.17265/1934-7375/2014.11.003

New Environmental Friendly Yellow Ceramic Pigments of the Type ($Fe^{III}M^{V}$)-TiO_2

Araceli Elisabet Lavat* and Griselda Xoana Gayo

CIFICEN (Centre of Investigations in Physics and Engineering of the Centre of Buenos Aires Province),CONICET-UNCPBA (National Council of Scientific and Technical Research, Faculty of Engineering, National University of the Centre of Buenos Aires Province), Olavarría B7400JWI, Argentina

Abstract: The family of Cr(III) and Fe(III)-doped rutile pigments of nominal composition $(M^{III}M'^{V})_xTi_{1-2x}O_2$, with M^{III} = Cr(III) or Fe(III) and M'(V) = Sb, Nb, Ta, with x = 0.03, 0.15 and 0.25 were investigated as ceramic pigments covering the yellow-ochre-brown palette. The formulations containing Fe(III) are novel compositions not included in the commercial rutile pigments. The materials were characterized by XRD (X-ray diffraction) analysis and FTIR (Fourier transformed infrared spectroscopy). The transition temperature from anatase-to-rutile was estimated by the evolution of the spectral patterns. This crystal phase transition is responsible of the color formation. A higher distortion of TiO_6 octahedra is observed in the case of (FeSb) containing cells which contribute to the enhancement of the light absorption. The coloring performance of all the formulations were evaluated by enameling the mixtures containing 5% pigments and commercial frits representative of single and double firing industrial processes. The chromatic values obtained are in the yellow to brown domain of the chromatic plot, depending on the composition of the pigment-frit batch. In the case of the Fe-glazes, and particularly the combination (FeNb), the chromatic values are close to the best yellow tinting. This new FeNb-rutile pigment could be a more benign substitute of Cr-yellow pigments. The homogeneity of the enamels was confirmed by SEM (scanning electron microscopy)-EDAX (energy dispersive X-ray analysis) microscopy.

Key words: ($Fe^{III}M^{V}$)-TiO_2, color, glassy coating, spectroscopy, X-ray methods, electron microscopy.

1. Introduction

Inorganic pigments have been used by mankind since early times for decoration purposes. Apart from providing color, ceramic pigments are required to be highly refractory, capable of withstanding the chemical corrosion of the liquid phases formed during the firing of bodies and glasses and displaying suitable optical properties.

These materials are widely applied by ceramic industries in the manufacture of sanitary and household ware, roof and floor tiles and glass. For these purposes, a high thermal and chemical stability is required, as well as color maintenance during enameling.

Although ceramic pigments are traditional materials, new systems that offer permanent opportunities are being researched. One of the major challenges in the field of ceramic pigments is to achieve difficult colors. This could be due to many reasons: discoloration for being unstable by firing at high temperature, high cost of fabrication, toxicity of the composing element, among others [1]. To overcome these limitations several strategies have been proposed, moreover, when pure oxides are used as pigments, only a narrow spectrum of colors are achieved, whereas in the modern synthesis of pigments many crystalline structures are involved and new palettes of colors with improved thermal resistance are produced [2].

There are several possibilities for many colors, such as blue, green, turquoise, brown, pink, but the palette of yellow-orange-red available is rather limited [3]. For example, a major concern for preparing a yellow tone is the purity of the color required. When only a

*Corresponding author: Araceli Elisabet Lavat, Ph.D., research fields: chemistry and ceramics. E-mail: alavat@fio.unicen.edu.ar.

moderately pure yellow is required, Zr-V-pigments are the adequate economic options since lemon to orange yellows are obtained. A more pure and stable yellow shade is achieved by using Sn-V-pigments although these are more expensive. The best bright pure yellow and high thermal resistance is obtained with Pr-doped zircon pigments. Furthermore, the strongest yellow is obtained with Cd sulfide and sulfoselenide but, due to the nonoxidic character, the pigment is not stable in the most common oxide based glazes.

However, in the last years, novel materials have been proposed. Perovskite based inorganic pigments (Ca, La)Ta(O, $N)_3$, depending on composition, have been reported as yellow through orange to deep red pigments, which became a promising benign replacement for toxic Cd-based materials that can adversely affect the environment and human health [4]. However, to improve their thermal resistance, the particles must be coated by refractory materials like zircon or zirconia.

Some other new safe improved inorganic yellow pigments have been reported. An example of this is $Ce_{1-x}ZrBi_yO_{2-y/2}$ solid solutions for ceramic applications. In addition, the particles can be obtained by citrate route synthesis under micron sizes suitable for the application in inkjet decoration [5]. New tungstate based ceramic pigments $Zn_xNi_{1-x}WO_4$ with wolframite structure, obtained by using a polymeric precursor, display yellow colour by increasing the amount of Ni [6].

On the other hand, doped titanates structures are among the materials that emerged as ceramic pigments. A yellow pigment with pyrochlore structure $Ca_xY_{2-x}V_xTi_{2-x}O_7$ has been known since 1993 as a substitute for the decreasing variety of available yellow ceramic pigments due to the secure regulations of toxic lead and cadmium. The synthesis of the related mixed oxide yellow hue has been reported [7]. The karrooite structure $MgTi_2O_5$ can host several transition metal cations in octahedral coordination giving rise to the development of different colors. In this way, doping with Ca is green, with Ni yellow and with Co, Cr, Fe, Mn and V, the colors range from orange to brown tan [8].

TiO_2 rutile is widely used as brilliant white pigment in paints, plastics, papers and foods. Due to its excellent optical properties, high melting point and capacity to develop intense coloration when doped with chromophores, it is applied as ceramic pigment [9, 10]. In fact, several industrial pigments are manufactured departing from the polymorph anatase by incorporation of colored oxides (Cr, Mn, Ni or V) and the counterions (Nb, Sb or W) necessary to compensate the cation charge imbalance due to substitution of Ti(IV) with mineralizers. Also, different precursor synthetic procedures of Cr, Sb-TiO_2 orange pigment have been applied to produce in situ colored ceramic bodies [9].

In view of the permanent interest in the development of new pigments covering the yellow-orange-red palette which meets the requirements for ceramic applications, the present study is focused on pigments based on the rutile structure. In order to get a deeper insight into this family of pigments, we have investigated the doped oxides $(M^{III}M'^{V})_xTi_{1-2x}O_2$, with M^{III} = Cr or Fe, and M'^{V} = Sb, Nb, Ta as counterions, with x = 0.03, 0.15 and 0.25. The role of the counterion is to balance the charge mismatch between Ti(IV) and the trivalent chromophores. The color of the pigments is achieved by firing at high temperature around 1,000 ^{o}C, and it is due to the incorporation of the chromophores into the rutile structure [11]. All the rutile doped oxides containing Fe(III) and the combination containing Cr/Ta are new formulations explored in this study to enlarge the palette of existing yellow-ochre-brown shades. TiO_2-rutile crystal lattice allows a wide degree of isomorphic substitution. Based on the fact that a continuous solid solution is expected, other nominal compositions not included in commercial pigment formulations, were investigated from the technological

point of view.

2. Experiments

The materials were prepared departing from TiO_2-anatase and the corresponding oxides and carbonates of the metal cations involved in each formulation, in stoichiometric proportion, using the traditional ceramic procedure. The mixtures of TiO_2, anatase (Aldrich, 99.9%), Fe_2O_3 (Riedel-de Haën 97%), Cr_2O_3 (BDH 99%), Sb_2O_3 (Riedel-de Haën 99.5%), Nb_2O_5 (Aldrich 99.9%) and Ta_2O_5 (Aldrich 99.9%) were prepared in order to achieve the nominal composition $(M^{III}M'^{V})_xTi_{1-2x}O_2$, x = 0.03, 0.15, 0.25. The starting mixtures were homogenized in an agate mortar and fired in platinum crucibles in a muffle electrical furnace for 2 h, with intermediate grindings. The heating rate was 10 ^{o}C/min and the pigments were calcined at 1,000 ^{o}C, reactions were carried out in air.

The synthesized mixed oxides were studied by XRD (X-ray diffraction) and FTIR (Fourier transformed infrared spectroscopy) analysis. X-ray diffraction patterns were obtained using a Philips PW 3710 diffractometer equipped with graphite monochromator, using CuKa radiation, and operating at 40 kV and 20 mA. The following X-ray data collection details were applied: slit divergence: (1/12)º, receiving slit: 0.2, step interval: 0.02°, time per step: 1 s.

The infrared spectra were recorded on a Nicolet-Magna 550 FT-IR instrument, using the KBr pellet technique. Unit cell parameters were obtained using a least-square procedure and refined with a locally modified version of the Werner PIRUM programme [12]. The XRD measurements were calibrated using Si as internal standard.

Prior to enameling the pigment and ceramic frit test, specimens were prepared by mixing thoroughly. The composition of the transparent frit, typically employed in the single firing process in roof and floor tiles manufacturing, is detailed in Table 1. The mixtures containing 5% pigment were homogenized in an agate mortar. Every bath was wet mixed and the slip was spread on porous ceramic tiles, then dried in air and finally submitted to thermal treatment. In some cases, cylindrical test specimens were formed by pressing at 416 MPa, the powder containing 0.06 kg H_2O/kg dry solid. The resulting materials were put onto ceramic biscuits and fired. The thermal cycles consisted in heating at 1,000 ^{o}C and 850 ^{o}C for SF (single firing) and DF (double firing), respectively. The pure frit was fired also at different temperatures for comparative purposes. All the samples were milled and characterized by XRD and FTIR. UV (ultraviolet)-visible spectroscopy measurements of powdered enamels were obtained by diffuse reflectance, with a Shimatzu UV-300 instrument model, using MgO as a standard. CIE (International Commission on Illumination) L∗a∗b∗ colour coordinates of coated tiles were obtained with a Braive Super Chroma 20 mm colorimeter and a white standard as reference. The microstructure of the glassy enameled tiles was obtained by SEM (scanning electron microscopy) using a Carl Zeiss, model MA10, microscope. The X-ray dispersive microanalysis was performed by EDAX (energy dispersive X-ray analysis) Orford equipment, model INCA Energy. The microstructure of the enamels was obtained on superficially polished gold-coated specimens.

3. Results and Discussion

3.1 Structural Features of the Cr and Fe-Pigments

The structure of rutile is tetragonal ($a = b$ = 4.594 Å and c = 2.959 Å), space group $P4_2/mmm$, formed by chains of slightly distorted TiO_6 octahedra (with two

Table 1 Approximate composition of transparent ceramic frit in oxides (wt.%).

Oxides (wt.%)	Na_2O	K_2O	CaO	MgO	PbO	B_2O_3	Al_2O_3	SiO_2
Frit A (DF)	2-3	1-3	3-5	-	28-32	4-6	4-6	48-50

Frit C (SF)	4-7	1-3	3-5	-	-	14-17	9-11	60-65
Frit D (SF)	9	9	10	10	-	8	8	65

long apical Ti-O bonds and four short apical Ti-O distances), sharing a vertex along the c axis. The interstices available in the "host lattice" allows the incorporation of almost every first row transition element and even of elements of further rows without compromising the structural integrity of the lattice.

The presence of the "guest" chromophores cations Fe(III) and Cr(III) must be accompanied with the pentavalent counterions Sb, Nb and Ta necessary to maintain the charge neutrality of the lattice. The development of color occurs during the anatase-to-rutile transition by firing at high temperature. This crystal transition is mainly influenced by the presence of the chromophores, by increasing the oxygen vacancies concentration, which tends to decrease the onset temperature. In the case of the Cr/Sb cation combination, the drop is as low as 300 ^{o}C under the undoped TiO_2 value [10, 11]. It is well known that, the transition temperature is also influenced by the occurrence of accessory phases containing chromophores and counterions (such as $CrSbO_4$), in the thermal range 700-1,000 ^{o}C. In some way, this accessory phases act as nucleation centers for anatase-to-rutile transition because they decompose by heating at a temperature higher than 1,000 ^{o}C, giving rise to rutile as a unique phase.

3.2 XRD Characterization of $(M^{III}M'^{V})_xTi_{1-2x}O_2$ Pigments

The X-ray powder diagrams of all the materials synthesized at 1,100 ^{o}C clearly confirm the presence of the tetragonal TiO_2-rutile. A typical example is shown in Fig. 1. The XRD pattern of the samples could be indexed based on the tetragonal rutile structure, PDF (powder difraction file) #211276. This confirms the isomorphic substitution by the incorporation of the MM' combination of doping cations in the rutile crystal network.

The calculated unit cell parameters are shown in Table 2 for some representative pigments of the family. According to the data of Table 2, the parameters $a = b$ are very close to those of pure rutile. However, in the case of the parameter c, higher values in comparison with the undoped cell are observed, in agreement with the larger sizes of the MM' cations combinations in comparison with Ti(IV). As it can be seen from Table 2, some trends could be found in doping. In both chromium and iron containing cells, the dependence of the lattice parameters from the dopant content x shows that $a = b$ decreases smoothly with decreasing substitution, whereas the c parameter shows the same trend for (CrSb) containing cells but an opposite trend in the case of (FeSb) and (FeTa) ones.

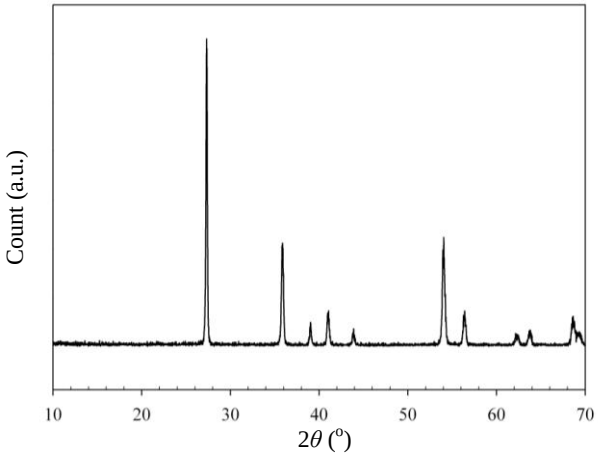

Fig. 1 XRD pattern of $(FeSb)_{0.25}Ti_{0.75}O_2$.

For a fixed x = 0.25 value, the comparison of the cell parameter variations with counterion sizes in the Cr and Fe-lattices shows, according to Table 2, that the parameter a remains practically invariant with cation substitution. In the case of the parameter c, it seems to be more influenced by the counterion and its variation follows the order: Sb > Nb ≈ Ta which is not in good agreement with the pentavalent cation radii. On the other hand, due to the higher polarizing effect of Sb(V), certain degree of covalency accompanied with the shortening of Sb-O bonds should be expected. The observed elongation of c axis in Sb

cells would account for the presence of Sb(III), as reported in Ref. [11].

On the other hand, these evidences suggest that, due to the apical Ti-O distances elongation, a higher distortion (higher *c*/*a* values) of octahedra is observed. This feature is particularly noticeable in the case of FeSb bearing materials which could contribute to the enhancement of the light absorption coefficient of d-d electronic transitions, responsible for the observed colour due to the reduction of the octahedral symmetry.

Table 2 Unit cell parameters and cell volumes of pigments.

Pigments $(M^{III}M'^{V})_xTi_{1-2x}O_2$ (colours)	Unit cell parameters (Å)		
	a = *b*	*c*	*c*/*a*
$(CrSb)_{0.25}Ti_{0.75}O_2$ (bright yellow)	4.597(7)	2.981(2)	0.648
$(CrSb)_{0.15}Ti_{0.85}O_2$ (bright yellow)	4.594(9)	2.972(8)	0.647
$(CrSb)_{0.03}Ti_{0.97}O_2$ (bright yellow)	4.593(0)	2.959(4)	0.644
$(CrNb)_{0.25}Ti_{0.75}O_2$ (dark brown)	4.598(5)	2.961(4)	0.644
$(CrTa)_{0.25}Ti_{0.75}O_2$ (ochre)	4.603(2)	2.970(1)	0.645
$(FeSb)_{0.25}Ti_{0.75}O_2$ (green yellow)	4.601(9)	2.991(8)	0.650
$(FeSb)_{0.03}Ti_{0.97}O_2$ (green yellow)	4.595(1)	2.996(0)	0.652
$(FeNb)_{0.25}Ti_{0.75}O_2$ (ochre)	4.614(4)	2.974(5)	0.644
$(FeTa)_{0.25}Ti_{0.75}O_2$ (ochre)	4.603(1)	2.966(2)	0.643
$(FeTa)_{0.03}Ti_{0.97}O_2$ (ochre)	4.594(8)	2.960(2)	0.644

Regarding the comparison of the materials with the same degree of doping and for Sb and Nb-bearing materials, the Fe-cells are larger than Cr-cells, which approximately correlate with the decrease of the cation sizes in the order high spin Fe^{3+} (0.785 Å) > Cr^{3+} (0.755 Å). In general, there is a fair correlation between the crystal radii of dopants and the cell dimensions. These XRD data give support to the solid solution formation within the substitution range, the ionic charge of cations and the distortion of some of the studied materials.

3.3 Spectroscopic Characterization of $(M^{III}M'^{V})_xTi_{1-2x}O_2$ Pigments

Once the materials were fully characterized by XRD diffraction, the FTIR spectra were recorded in order to complete the structural characterization. Fig. 2 shows the spectral pattern of a representative sample.

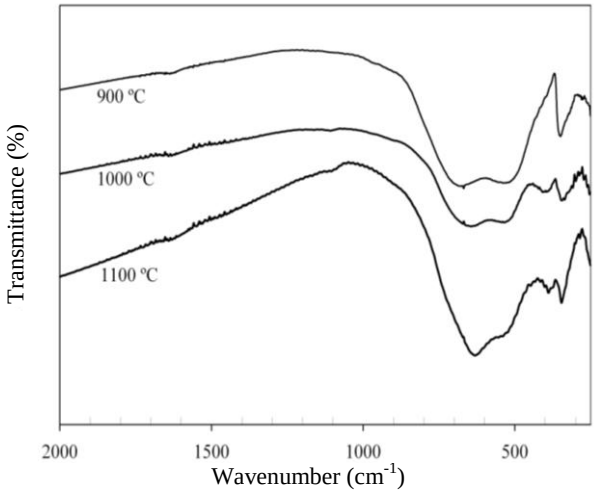

Fig. 2 Evolution of FTIR spectra of $(FeNb)_{0.25}Ti_{0.75}O_2$ at different temperatures.

The IR (Infrared) spectra of all the investigated materials show a similar distribution of their absorption bands. In this isostructural family of doped compounds, the different coordination polyhedra behave as coupled vibrational units forming the octahedral MO_6 chains. In this way, four absorption

regions lying in the spectral range from 690 cm^{-1} to 340 cm^{-1} are observed, similar to undoped TiO_2-rutile. However, considering the low degree of substitution of the phases, the main absorptions should be related to Ti(IV)-O bonds. These bonds are expected to be somewhat stronger than Cr(III)-O or Fe(III)-O bonds and weaker than the counterions M(V)-O.

The spectral pattern was assigned, according to the IR data available in Ref. [13], by comparison with related systems belonging to rutile structure. The sharp band lying at the highest frequency v_1 is attributed to the stretching of M-O-M bridge bonds. The following band v_2 (or shoulder) should be assigned to Ti-O stretching coupled with M-O and M'-O bonds from chromophores and counterions forming the octahedral chains. The remaining two absorptions ν_3 and ν_4 located at lower energies belong to the deformational modes O-M-O of the same polyhedra (O-Ti-O, O-M-O and O-M'-O).

The exact positions of all the investigated materials are presented in Table 3. The typical absorptions frequencies of rutile are included for comparison. The band positions in both Cr and Fe-containing solid solutions detailed in Table 3 seem not to follow a clear trend neither with the mass nor with the sizes of the counterion M'. All the bands are mixed character. Nevertheless, in the Sb-containing materials the bands are shifted to higher wavenumbers and approach those of undoped TiO_2. This seems to be related to the covalency of Sb-O bonds which contribute to the reinforcement of the other linked polyhedra. It also implies an increase of the solid stability.

Conversely, in the solid of the series (CrSb) with different compositions (x), this shows that with increasing degree of (CrSb) incorporation into the lattice, the absorption bands are shifted towards higher wavenumbers. Furthermore, the stretching frequencies are below the frequencies observed for isostructural completely substituted phase $CrSbO_4$, whereas the opposite trend was found in the case of deformation bands. A similar behavior is observed when $(CrTa)_{0.25}Ti_{0.75}O_2$ and $CrTaO_4$ are compared.

The FTIR spectra of the reaction mixture, thermally treated at different temperatures from ambient to 1,150 °C, were recorded in order to evaluate the evolution of the anatase-to-rutile transition with respect to the undoped titania, which occurs at 1,100 °C. Rutile and anatase are distinguishable by vibrational spectroscopy. Anatase is recognized by the medium intensity band located at 356 cm^{-1} and a strong, broad doublet with maximums at 590 cm^{-1} and 645 cm^{-1} which are assigned to deformational and stretching modes of O-Ti-O of the distorted TiO_6 octahedra constituting the structural building units of this solid [14].

The presence of rutile is noticeable by the pair of bands in the low energy region of the spectrum at 350 and 425 cm^{-1}, differentiable from anatase which shows a single band in this region (at 356 cm^{-1}), and also by the change of shape and shift to higher frequency of the broad absorption assigned to Ti-O stretching vibration due to the change of symmetry of TiO_6 polyhedra. According to the evolution of the spectra depicted in Fig. 2 registered during the formation of

Table 3 Observed FTIR frequencies of pigments.

Pigments $(M^{III}M'^{V})_xTi_{1-2x}O_2$	Band positions in (cm^{-1})				T (°C) A → R
	v_1	v_2	v_3	v_4	
$(CrSb)_{0.25}Ti_{0.75}O_2$	690	568	400 (393)	347 (340)	900
$(CrSb)_{0.15}Ti_{0.85}O_2$	677	546	354	338	-
$(CrSb)_{0.03}Ti_{0.97}O_2$	638	554	415	354	-
$(CrNb)_{0.25}Ti_{0.75}O_2$	649	544	408	342	1,000
$(CrTa)_{0.25}Ti_{0.75}O_2$	667	549	413	341	1,000
$(FeSb)_{0.25}Ti_{0.75}O_2$	673 (664)	585	396 (387)	341	850

$(FeNb)_{0.25}Ti_{0.75}O_2$	631	538	389	346	950
$(FeTa)_{0.25}Ti_{0.75}O_2$	630	528	391	345	950
TiO_2	680	610	425	350	1,100

$(FeSb)_{0.25}Ti_{0.75}O_2$ oxide, the typical spectrum of rutile is clearly observed at 1,000 °C (the persistence of anatase up to 950 °C), which means a drop of 150 °C in comparison with anatase-to-rutile transition from the undoped material. The analysis of spectral data of the samples calcined in the same thermal range was carried out and the estimated transition temperatures determined are shown in Table 3. According to Table 3, in both Cr and Fe-doped series, the lowering of the onset temperature follows the ordering: Sb < Nb ≈ Ta. In addition in Fe-bearing pigments, the transition temperature is approximately 50 °C lower than in Cr-oxides suggesting that iron pigments could be obtained at a lower temperature, implying an energy saving.

On the other hand, the color virage during the crystal phase transition is remarkable. In the case of Cr(III) containing materials, the change from green to bright yellow or brown, depending on M^V metal cation, confirms the incorporation of the chromophore to the rutile lattice.

3.4 Technological Properties and Colorimetric Characterization of Enamels

The colorimetric parameter measurements were performed on white ceramic biscuits enameled by adding 5% pigment to transparent frits commonly used for single firing (C and D) and double firing (A) obtained at 1,000 °C and 850 °C, respectively, in applications regarding ceramic tiles and sanitary wares. As can be observed in Figs. 3 and 4, the FTIR spectral patterns of the glazes based on frits A and C are conserved. These suggest that the glassy boro-silicate network remains unchanged during the enameling process.

The morphology of the enamels obtained with DF and SF frits are depicted in Figs. 5 and 6. The SEM micrographs show a homogenous microstructure free of surface defects. Moreover, the EDAX microanalysis demonstrates that the global composition of the enamels is consistent with the composition of pigment-frit batches.

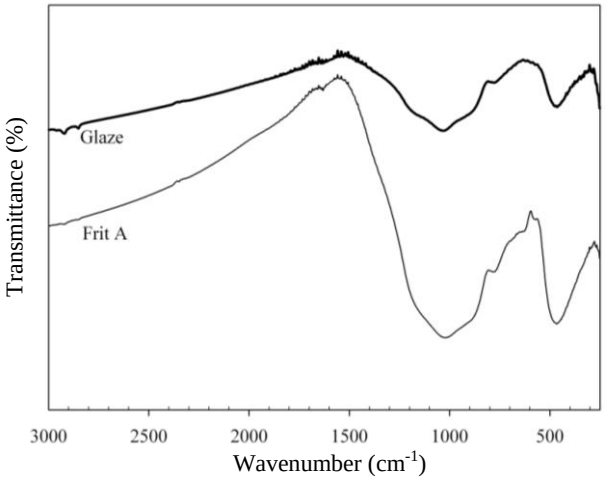

Fig. 3 FTIR spectra of $(FeSb)_{0.25}Ti_{0.75}O_2$ pigment glazed with frit A, at 850 °C.

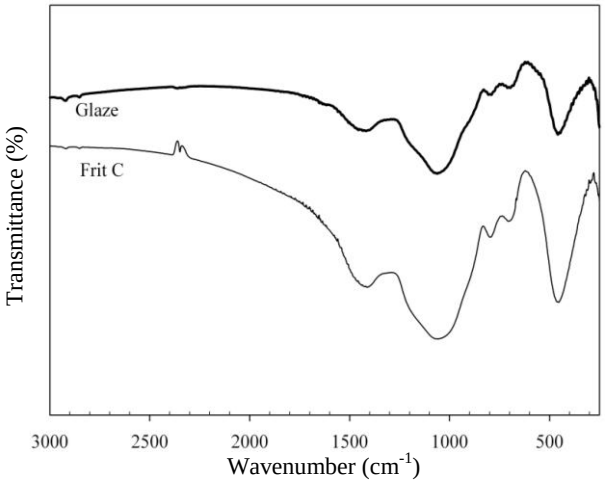

Fig. 4 FTIR spectra of $(CrNb)_{0.25}Ti_{0.75}O_2$ pigment glazed with frit C, at 1,000 °C.

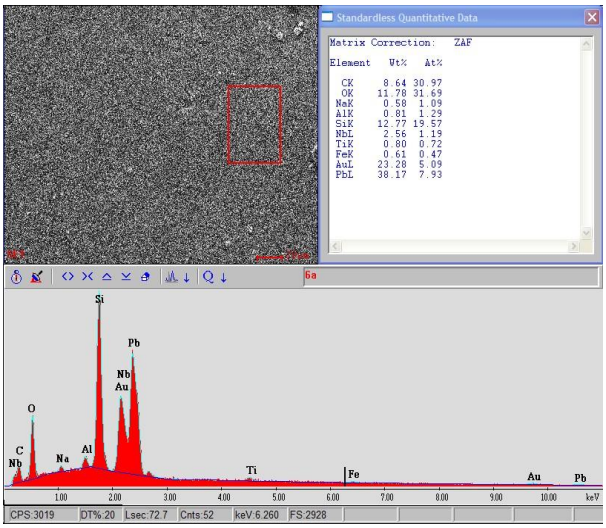

Fig. 5 SEM micrograph and element composition of $(FeNb)_{0.25}Ti_{0.75}O_2$, enamelled with frit A.

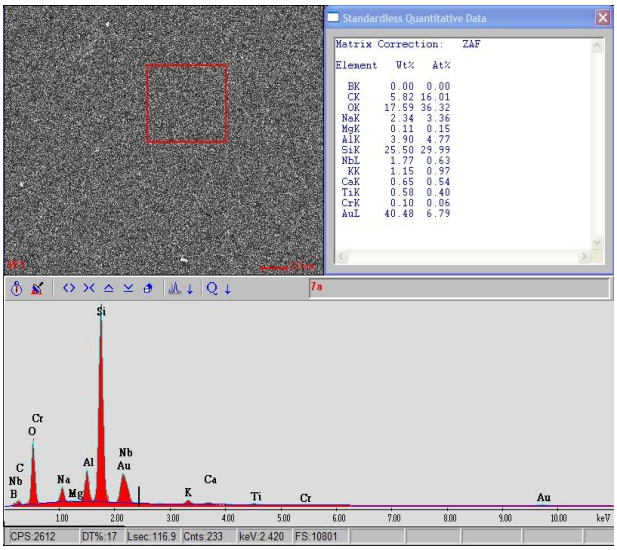

Fig. 6 SEM micrograph and element composition of $(CrNb)_{0.25}Ti_{0.75}O_2$, enamelled with frit C.

The resulting CIELab parameters of all the specimens are detailed in Table 4. The colorimetric properties of the pigments are fairly maintained after the glazing at high temperature, depending on the frit and thermal treatment. As it can be observed in Table 4, the presence of the counterions modifies the coloring properties of the M(III) chromophores. According to the values of lab, the coatings are in the domain of yellow, ochre and brown region, characterized by $+a/+b$ chromatic values.

The colours of these pigments are determined by both metal-ligand charge transfer from $Ti^{4+} \leftarrow O=$ and crystal field effects of the transition metal chromophores in octahedral coordination [10]. During the calcination of the pigments, a shift towards visible light is produced by the transformation of anatase-to-rutile. On the other hand, an enhancement of d-d electronic transition of d^3 and d^5 electrons belonging to Cr^{3+} and Fe^{3+}, respectively, occurs once these cations incorporate to rutile lattice, giving rise to bands in the electronic spectra of the pigments [10].

In the case of Cr(III)-earing pigments enameled with frit C, when Sb is the counterion the CIELab values are located close to the typical region of Cr-Ti maple pigments, particularly for the low substitution material which also shows the highest *L* value, as expected. For the other counterions Nb and Ta, enameled with frit C, are clearly brown shades, with the chromatic values similar to those of Zr titanate pigments [15] and also to CrFeZnAl-spinel brown commercial pigments. For the double firing glazes prepared with Cr(III) pigments with $x = 0.25$, despite of the counterion, these show CIELab parameters $+b$ which are over the ZrV-yellow region of the chroma plot.

Regarding Fe(III) glazes, according to Table 4, the highest $+b$ yellow chroma is achieved particularly for double firing application. The CIELab values show the highest $+b$ values and simultaneously the lowest $+a$ of the series. The chromatic values are better than ZrV-yellow industrial pigments and in the case of the combination FeNb, the values get closer than the rest of the materials to the Ref. [3] pigment $ZrSiO_4$: Pr-yellow chroma, which is the best tinting strength (brightest and purest yellow). As a consequence, this new FeNb-rutile pigment could be a more benign and low cost substitute for the pigments of this system, particularly for those containing the combination Cr/Sb, which are more toxic. In the case of Fe/Ta, the value of $+a$ and $+b$ coordinates seem to be more sensible to the degree of doping since it decreases with the decreasing of *x*.

Finally, as it can be seen in Table 4 when the

Fe(III)-0.25 pigments are incorporated to another ceramic glaze used in single firing, the chromatic values obtained are in the yellow-brown domain of the chroma plot.

4. Conclusions

New formulations of Cr and Fe-doped rutile pigments, not included in commercial pigments, were explored in order to enlarge the palette of yellow to brown shades. The synthesis of these rutile pigments was carried out by solid state reactions at high temperature, involving the formation of secondary phases $MM'O_4$ (e.g., $CrSbO_4$) and the crystal transition from anatase-to-rutile. The color formation is facilitated by the diffusion of chromophores into the octahedral site of rutile structure.

Table 4 CIELab parameters of glazes based on frits A (DF), C and D (SF).

Pigments	SF: frits C and D			DF: frit A		
	L	*a*	*b*	*L*	*a*	*b*
$(CrSb)_{0.25}Ti_{0.75}O_2$	48.77	11.06	35.53	46.13	9.01	35.53
$(CrSb)_{0.15}Ti_{0.85}O_2$	43.59	11.02	29.26			
$(CrSb)_{0.03}Ti_{0.97}O_2$	60.71	12.54	36.99			
$(CrTa)_{0.25}Ti_{0.75}O_2$	46.02	3.73	16.35	39.07	11.57	43.82
$(CrNb)_{0.25}Ti_{0.75}O_2$	41.36	12.09	18.35	31.70	7.78	34.45
$(FeSb)_{0.25}Ti_{0.75}O_2$	79.45	3.70	23.20	67.64	3.78	51.23
$(FeNb)_{0.25}Ti_{0.75}O_2$	72.77	10.02	36.09	63.74	2.17	46.42
$(FeTa)_{0.25}Ti_{0.75}O_2$	71.23	8.45	31.59	58.11	4.11	40.04
$(FeSb)_{0.03}Ti_{0.97}O_2$				68.49	-3.33	33.83
$(FeTa)_{0.03}Ti_{0.97}O_2$				67.46	2.09	34.72

XRD data confirm the solid solution formation. In general, Fe-cells are larger than Cr-cells in accordance with cation sizes in octahedral sites. In addition, the larger *c*/*a* values which reflect the apical Ti-O bond length and octahedral distortion were observed in (FeSb) containing materials.

The transition temperature of anatase-to-rutile was estimated by the evolution of FTIR spectra of the phases thermally treated up to 1,100 ^{o}C. In both Cr and Fe-doped series, the lowering of the onset temperature is: Sb < Nb ≈ Ta. In addition, the transition temperature is approximately 50 ^{o}C lower in Fe-containing pigments in comparison with Cr-oxides. This implies that the synthesis of iron pigments could be achieved at lower temperature than chromium pigments with consequent energy saving.

According to CIELab colorimetric values, a palette of yellow to brown is obtained using Cr and Fe pigments for single firing procedures. In double firing applications, all the Fe-containing glazes show the best yellow chromatic values, in brightness and purity. Particularly the combination (FeNb) represents a new and very interesting Cr-free and lower cost yellow pigment for low temperature applications.

Acknowledgments

This work was supported by UNCPBA (National University of the Centre of Buenos Aires Province) and CONICET (National Council of Scientific and Technical Research, Faculty of Engineering, National University of the Centre of Buenos Aires Province). The authors would like to thank to Ing. Noelia López for colorimetric measurements.

References

[1] Viswanath, N. Ceramic Pigments. *Ceram. Ind.* **2010,** *160,* 23-25.

[2] Xanthopoulou, G. Self-Propagating SHS of Inorganic Pigments. *Am. Ceram. Soc. Bull.* **1998,** *7,* 87-96.

[3] Eppler, R. Selecting Ceramic Pigments. *Ceram Bull*. **1987,** *66,* 1600-1604.

[4] Jansen, M.; Letschert, H. P. Inorganic Yellow-Red Pigments without Toxic Metals. *Nature* **2000,** *404,* 980-982.

[5] Furukama, S.; Masui, T.; Imanaka, N. New

Environment-Friendly Yellow Pigments based on CeO_2-ZrO_2 Solid Solutions. *J. Alloys Compd*. **2008,** *451*, 640-643.

[6] de Oliveira, A.; Jailson, M.; Ferreira, M.; Silva, M.; Braga, G.; Soledade, L.; et al. Yellow $Zn_xNi_{1-x}WO_4$ Pigments Obtained Using a Polymeric Precursor Method. *Dyes and Pigments* **2008,** *77*, 210-216.

[7] Gargori, C.; Galindo, R.; Cerro, S.; García, A.; Llusar, M.; Monrós, G. Synthesis of a New $Ca_xY_{2-x}V_xSn_{2-x}O_7$ Yellow Pigment. *Phys. Proc.* **2010,** *8*, 84-87.

[8] Matteucci, F.; Cruciani, G.; Dondi, M.; Gasparotto, G.; Maria, T. D. Crystal Structure, Optical Properties and Colouring Performance of Karrooite $MgTi_2O_5$ Ceramic Pigments. *J. Sol. St. Chem*. **2007,** *180*, 3196-3210.

[9] Gargori, C.; Cerro, C.; Galindo, R.; Monrós, G. In Situ Synthesis of Orange Rutile Pigments by Non-conventional Methods. *Ceram. Int.* **2010,** *36*, 23-31.

[10] Matteucci, F.; Cruciani, G.; Dondi, M.; Raimondo, M. The Role of Counterions (Mo, Nb, Sb, W) in Cr-, Mn-, Ni- and V-Doped Rutile Ceramic Pigments Part 1, Crystal Structure and Phase Transformations. *Ceram. Int.* **2006,** *32*, 385-392.

[11] Matteucci, F.; Cruciani, G.; Dondi, M.; Raimondo, M. The Role of Counterions (Mo, Nb, Sb, W) in Cr-, Mn-, Ni- and V-Doped Rutile Ceramic Pigments Part 2, Colour and Technological Properties. *Ceram. Int.* **2006,** *32*, 393-405.

[12] Werner, P. E. FORTRAN Program for Least-Squares Refinement of Crystal Structure Cell Dimensions. *Ark. Kemi*. **1969,** *31*, 513-516.

[13] Filipek, E.; Dabrowska, G. New Solid Solution $Fe_{1-x}Cr_xVSbO_6$ with Rutile-Type Structure. *J. Alloys Compd.* **2012,** *532*, 102-107.

[14] Chatterjee, S.; Bhattacharyya, K.; Ayyub, P.; Tyagi, A. K. Photocatalytic Properties of One-Dimensional Nanostructured Titanates. *J. Phys. Chem. C* **2010,** *114*, 9424-9430.

[15] Dondi, M; Matteucci, F.; Cruciani, G. Zirconium Titanate Ceramic Pigments: Crystal Structure, Optical Spectroscopy and Technological Properties. *J. Solid St. Chem.* **2006,** *179*, 233-246.